 Cytometry 31:287–294 (1998)

Automated Image Analysis System for Detecting Boundaries of Live Prostate Cancer Cells

Inpakala Simon,[1] Charles R. Pound,[1] Alan W. Partin,[1] James Q. Clemens,[1] and William A. Christens-Barry[2]*

[1]James Buchanan Brady Urological Institute, The Johns Hopkins Hospital, Baltimore, Maryland
[2]The Johns Hopkins University Applied Physics Laboratory, The Johns Hopkins University, Baltimore, Maryland

Received 26 June 1997; Accepted 2 December 1997

Image analysis provides a powerful tool for quantifying cell motility and has been used to correlate motility with metastatic potential in an animal model of prostate cancer. However, widespread use of this image analysis method has been limited because earlier methods of quantitative analysis required time-intensive and subjective manual tracing of cell contours. In this report, we describe a fully automated image segmentation algorithm for detection and morphometric description of prostatic cells. The segmentation system was tested on prostate cell images generated from Hoffman modulation contrast microscopy (47 cells at 64 time points = 3,008 images) and differential interference contrast microscopy (29 cells at 64 times points plus 1 cell at 62 time points = 1,918 images). Morphometric measurements were derived from computer-determined cell boundaries and compared with the same measurements derived from manually traced cell boundaries. Final correlation coefficients for area and perimeter measurements for Hoffman and differential interference contrast microscopy were (0.76, 0.62) and (0.93, 0.93), respectively. Results with our differential interference contrast images demonstrate that our segmentation algorithm reliably and efficiently replaces the need for manually traced cell boundaries in addition to eliminating intraobserver variation. Our automated segmentation process will have immediate utility in our motility analysis system that relates cell motility with metastatic potential of prostate cancer. Cytometry 31:287–294, 1998.

Key terms: prostate; cancer; cell; microscopy; image segmentation; motility; morphometry

Prostate cancer is the most commonly diagnosed cancer and the second leading cause of cancer-specific death among men in the United States (16). In 1997 alone, more than 334,000 new cases of prostate cancer were diagnosed and more than 41,000 prostate cancer deaths occurred (16). Prostate cancer is unusual in that it is a common disease in elderly men, but only behaves as an aggressive, potentially lethal cancer in certain individuals.

For many years, research efforts have been focused on accurate methods of differentiating indolent from more aggressive cancers. Since the original description by Gleason (5) of a pathologic grading system, other methods of predicting cancer aggressiveness, using nuclear morphometry as well as various molecular markers which include DNA ploidy (4), Ki-67 (1), and p53 (25), have been reported. These methods have been based primarily on the analysis of fixed, histologic sections of prostate cancer. By concentrating research efforts solely on the analysis of nonliving tissue, we are ignoring certain aspects of prostate cancer that may be important in determining the metastatic potential of individual tumors.

Dynamic analysis of live cells to quantify various motility characteristics has been instrumental in understanding ciliary function (11), cell development (28), early physiologic cellular reactions (26), nuclear organization (10), cytoplasmic forces (9), neuronal death (3), and the metastatic potential of animal models of prostate cancer (14, 17). Common methods of imaging these cells for motility analysis have been brightfield, fluorescence, phase contrast, modulation contrast, and differential interference contrast microscopy (6). Not all of these imaging modalities are optimal for live prostate cells. For instance, the transparency of cells often leads to low-contrast images if brightfield microscopy is used. Vital dyes have the potential for influencing cell motility processes and decay of the

Contract grant sponsor: NIH; Contract grant number: SPORE CA58236.
Present affiliation for James Q. Clemens is the Department of Urology, Northwestern University Medical School, Evanston, Illinois.

*Correspondence to: William A. Christens-Barry, The Johns Hopkins University Applied Physics Laboratory, Johns Hopkins Rd., Laurel, MD 20723-6099.

E-mail: wacb@aplcomm.jhuapl.edu

signal occurs rapidly, thus limiting the extent to which fluorescence microscopy can be employed to quantify cell motility. Phase contrast techniques accentuate the boundaries of flat surfaces of prostate cells with a white ''halo,'' creating an artifact that interferes with further analysis of cell shape (8,20). In consequence of these shortcomings, modulation contrast (Hoffman) and differential interference contrast (DIC) microscopy are often used to achieve high-contrast images of motile prostate cells (13,14,19).

Hoffman microscopy detects optical density gradients using a spatially varying transmittance filter (modulator). This filter causes the modulation of opposite gradients above and below average background intensity, which produces a three-dimensional appearance to a cell image (8). DIC microscopy also gives a three-dimensional appearance to a cell's image, but does so by using birefringence optics consisting of Nomarski prisms and a polarizer (6,8).

Live cell boundary detection, i.e., image segmentation, is a central requirement of any quantitative motility analysis. Special attributes of Hoffman and DIC images undermine the use of segmentation techniques that have been developed for analysis of brightfield and fluorescence images. For example, the intensity of cell borders in Hoffman images can be lighter or darker (or both) than the surrounding background intensity (asymmetric intensity border), which makes segmentation difficult (8). DIC images place an even greater demand on segmentation algorithms due to their resolution of common delicate cell components (e.g., membrane ruffles, pseudopodal extensions, undulations) in addition to the asymmetric intensity borders (8,20,24). As a result, effective use of Hoffman and DIC images requires modification of many segmentation techniques, including image thresholding (7,23), first- and second-order statistical analyses (27), B-splines (10), color feature analysis (21), and fractal features (2). In order to segment the borders of cultured cells in Hoffman and DIC images, we developed specialized algorithms that could be utilized in an automated system for performing cell motility and morphometry analyses.

Our focus has been on the use of segmented cell information in the prediction of metastatic potential of rat prostatic adenocarcinoma cell lines (12–14,18–20). Previously, Partin et al. (19) developed a Fourier analysis method that used a sequence of spatial and temporal Fast Fourier Transforms to describe quantitatively the cell's dynamic shape change, based on temporal alterations in the boundary. This Fourier analysis scheme was applied to in vitro cells from low and high metastatic Dunning sublines of the rat prostatic adenocarcinoma (19). This study showed a strong correlation between the calculated Fourier measurements and metastatic potential. Widespread use of this Fourier methodology has been partially limited because earlier quantitative analyses required time-intensive and subjective manual tracing of cell boundaries from microscopic images. To eliminate the tedious process of manual cell tracing, we developed a segmentation algorithm for a cell motility analysis system. This approach has the further benefit of providing an objective, reproducible method of determining cell boundaries for our motility system and for other systems involving cell image analysis.

In this paper, we examine the segmentation of cultured motile prostate cells, imaged using both Hoffman and DIC video microscopy. Features are extracted from segmented cell boundaries and used to characterize the morphometry of these motile cells, which can be utilized in prostate cancer research. Features extracted from cell boundaries derived using our segmentation algorithms are compared with those derived from manual cell tracings.

MATERIALS AND METHODS

Culture and Video Microscopy of Cells (Hoffman Microscopy)

Cells from the highly metastatic MAT-LyLu subline of the Dunning R3327 rat prostatic adenocarcinoma were inoculated at low density ($\sim 10^5$ cells) on 25 cm^2 plastic tissue culture flasks. The cells were then equilibrated in 5% CO_2/95% air at 37°C in RPMI media containing 2 mM L-glutamine, 10% fetal bovine serum, 250 nM dexamethasone, penicillin G (100 units/ml), and streptomycin (100 units/ml). At 12–48 h after passage, these flasks were transferred to a 37°C-heated microscope stage for time-lapse video microscopy.

Forty-seven motile cells were viewed and manually focused (Hoffman modulation contrast optics) using an inverted Zeiss IM35 microscope (Carl Zeiss, Inc., Thornwood, NY) at 400× magnification (40× objective, 10× eyepiece) and a Hamamatsu C2400 video camera (Hamamatsu Photonics, Hamamatsu City, Japan). Images (N = 3,008) were captured using a raster graphics adapter (Data Translation Inc., Marlboro, MA) and commercially available software (DynaCELL, JAW Assoc. Inc., Annapolis, MD). Data Translation software compensated for the 4:3 aspect ratio of the Hamamatsu video camera. A series of 64 images was acquired over a period of 64 min by capturing images (size of 512 × 512 pixels) at 60-s intervals for each of the 47 cells. Using specialized software (NIH Image, developed by National Institutes of Health, Bethesda, MD), a smaller 64-image sequence was generated for each cell, the size of which was predetermined so that all cell movement would remain in the image.

Culture and Video Microscopy of Cells (DIC Microscopy)

Cells from Dunning R3327 rat prostatic adenocarcinoma sublines (AT2, AT3, G, MAT-Lu, and MAT-LyLu) were inoculated at low density ($\sim 10^5$ cells) onto 25 × 56 mm Lab-Tek TM chambered coverglass slides (Nunc, Inc., Naperville, IL) and equilibrated in conditions stated above, with the addition of fungizone to the RPMI media (0.250 mM). These sublines span the metastatic range of those used in previous studies of prostate cancer motility (19).

Thirty motile cells were viewed and manually focused (Nomarski optics) with a Zeiss Axiovert 35 inverted

microscope (Carl Zeiss, Inc.) at 400× magnification (40× objective, 10× eyepiece) and a CCD camera (C2400-600, Hamamatsu Photonics, Hamamatsu City, Japan). Images were captured (size of 640 × 480 square pixels) and digitized at a rate of 1 frame/min (N = 1,918, one cell had 62 frames) on a MacOS PowerPC (Power Computing Corp., Round Rock, TX) using an LG-3 Scientific Frame Grabber (Scion Corporation, Frederick, MD). A smaller 64-image sequence was generated for each cell in a manner identical to that used for Hoffman image sequences.

Manual Segmentation

A single investigator manually traced the cell contained within each 64-image sequence. The precision and accuracy of manual tracings were confirmed using calibrated size standards (polystyrene microspheres, average area of 78 ± 1.9 μm^2; Duke Scientific Corp., Palo Alto, CA). These standards were imaged using both Hoffman and DIC microscopy. For Hoffman microscopy, manual tracing yielded an average area of 73 ± 3.3 μm^2 (coefficient of variation, 4.5%). Manual tracing of spheres imaged using DIC microscopy gave an average area of 69 ± 2.9 μm^2 (coefficient of variation, 4.2%). Low coefficient of variation values demonstrate consistency in the manual tracing of standard objects.

For Hoffman images, the boundary of the cell in each recorded image of the 64-image sequence was manually outlined with a digitizer tablet (SummaSketch MM-1201, Summagraphics Corp., Fairfield, CT); XY coordinates of the points comprising the boundary were recorded using commercially available software (DynaCELL, JAW Assoc. Inc.).

For DIC images, manual tracing of cell boundaries was performed by a single investigator. Using NIH Image, each 64-image sequence was displayed on a computer screen. An outline around each cell was manually traced onto the image with a mouse. Once the outline was stored, the remaining 63 frames were sequentially accessed and analyzed.

Automated Segmentation Algorithm

Cell images that underwent manual tracing were reprocessed by our image analysis system for automatic detection of their boundaries. Image detection in our system consists of three major processes: noise reduction, unipolar intensity transformation, and edge detection. Modifications were made in the segmentation algorithm for DIC microscopy in order to address its ability to resolve delicate cell structures.

Hoffman Microscopy

The sequence of segmentation operations used to segment Hoffman images is illustrated in Figure 1. A 3 × 3 median filter was applied to the raw image to remove the high spatial frequency (single pixel) noise that dominated the image's noise spectrum (22). Unipolar intensity transformation of these median-filtered images was then accomplished using the following sequence of operations: (1) The mean grayscale of Figure 1a was subtracted, resulting in an image containing positive deviations from the mean (Fig. 1b); (2) Figure 1a was duplicated and its intensity values were inverted. Negative deviations from the mean were then retrieved (Fig. 1c); and (3) Figure 1b and Figure 1c were added to generate an image that gives the same value to equal positive and negative deviations, thereby making the image unidirectional or unipolar (Fig. 1d).

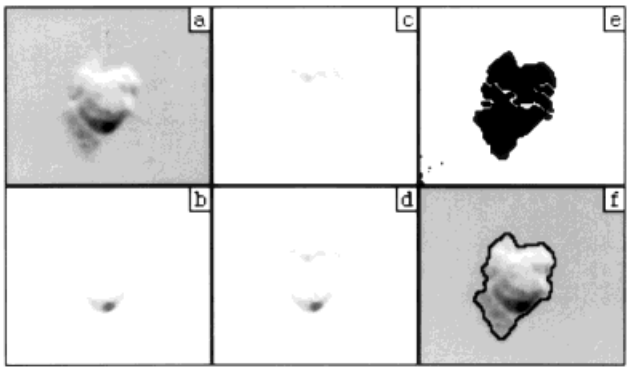

FIG. 1. **a:** Median-filtered Hoffman image of a prostate cell. **b:** Median image scaled to its mean intensity. **c:** Inverted median image scaled to its mean intensity. **d:** Unipolar intensity image of the prostate cell. **e:** Binary version of the unipolar intensity image. **f:** Outlined cell after a predetermined area threshold.

The transformation into unipolar intensity images was necessary to highlight cell images from the background, using global thresholding at the mean intensity (22). Segmented areas in the background image were eliminated using a preestablished area threshold (203 μm^2) based on the range of actual prostatic cell sizes observed in our data (Fig. 1e). Any holes within the segmented objects were filled in order to better estimate their areas. Final outlines were constructed from the filled segmented objects and traced on the original images (Fig. 1f). Area and perimeter measurements were computed for the manually- and computer-determined cell boundaries using a spatial calibration of 0.567 μm per pixel (Fig. 1).

DIC Microscopy

Segmentation of DIC images was based on the same approach developed for segmenting Hoffman images. Certain modifications were made in the algorithm to account for the ability of DIC microscopy to resolve fine cell structures. These modifications are illustrated in Figure 2 and described below.

First, since there were fewer high-frequency components, it was not necessary to perform noise reduction on DIC images. The original images (Fig. 2a) underwent unipolar transformation and global thresholding (Fig. 2b).

Secondly, small segmented areas in the background image were removed from the images (Fig. 2c) using NIH Image erosion and dilation operations in succession (15). In order to decrease the likelihood of extracting large structures that were touching the cell and the edge of the

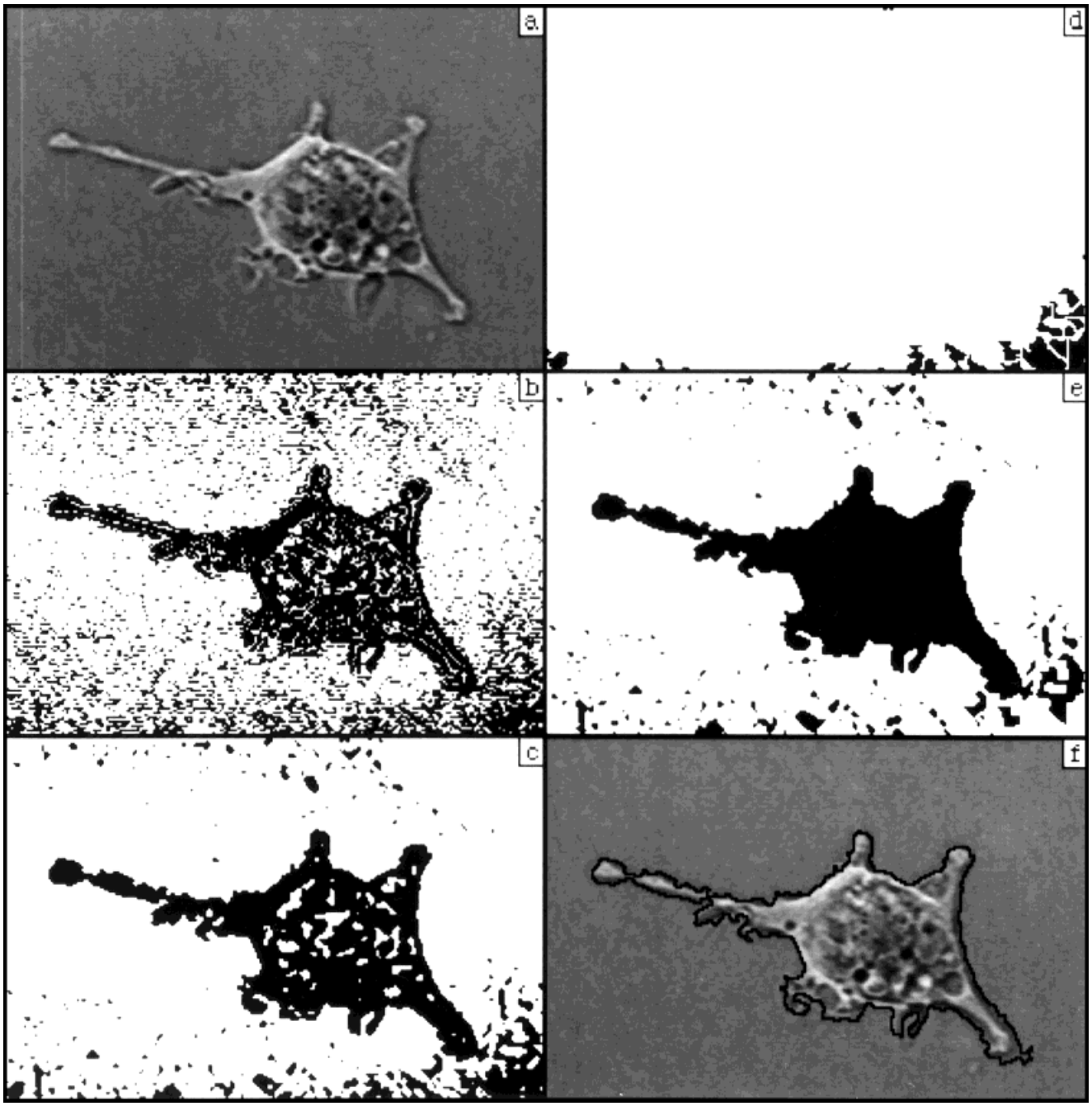

FIG. 2. **a:** Original DIC cell image. **b:** Image after unipolar intensity transformation and global thresholding. **c:** Removal of minute background structures using grayscale operations. **d:** Watershed procedure on objects touching the image edge. **e:** Rejoined image using rank filters with removal of objects touching the image edge. **f:** Outlined cell using largest area threshold.

image, watershed segmentation was performed on objects touching the image edge (Fig. 2d). Watershed segmentation is a method that separates touching but mostly convex objects in an image (22). This procedure is based on the premise that eroding a binary image will cause objects that are touching to separate before they disappear (22). This type of extraction allowed background regions touching the image edge to be ignored, thereby decreasing the number of candidate regions of the object (Fig. 2e). Regions were rejoined using standard maximum and minimum rank filters in succession (22). The region having the largest area within the image is representative of the

cellular area. This region was extracted, and the cell outlines were stored (Fig. 2f).

Area and perimeter measurements were computed for manually- and computer-determined cell boundaries using a spatial calibration of 0.285 μm per pixel. Cell images lacking adequate intensity contrast, i.e., cells with thin membranes, were excluded from further correlation analysis because sufficient intensity contrast is required for the algorithm to distinguish cell area from background area.

RESULTS

Figures 1 and 2 show the generation of cell outlines determined by the segmentation algorithms for Hoffman and DIC images. As an initial quantitative assessment of segmentation algorithm performance, area and perimeter measurements from computer derived cell boundaries were compared to those calculated from manually traced cell boundaries, with the assumption that manually traced boundaries are the gold standard.

For Hoffman images (N = 3,008), the correlation coefficients (Γ) for area and perimeter were 0.57 and 0.56, respectively. Poor segmentation resulted in unusually large calculated areas in some cell images having intensity bands similar to those of the background image. These intensity bands caused either inaccurate estimation of the actual area and of perimeter measurements or segmentation of the cell into two independent objects. When cell images with such unusually large calculated areas (e.g., >900 μm^2) were excluded (N = 15 cells) from statistical analysis, the correlation coefficients for area and perimeter improved to $\Gamma = 0.75$ and $\Gamma = 0.62$, respectively.

In DIC microscopy, area and perimeter measurements from computer-derived cell boundaries were compared to those calculated from manual cell tracings (Fig. 3). For all cells (N = 1,918), the correlation coefficients for area and perimeter were $\Gamma = 0.69$ and $\Gamma = 0.86$, respectively. When the analysis excluded a small fraction of cells whose images (320 images representing 5 cells) lacked adequate intensity contrast, correlation coefficients for area and perimeter improved to $\Gamma = 0.93$ and $\Gamma = 0.93$, respectively.

DISCUSSION

The developed segmentation algorithms were successful in segmenting Hoffman and DIC images. Though Hoffman and DIC morphometric feature analysis produced good correlations between manually- and computer-derived cell boundaries, segmentation using Hoffman images did not perform as well as segmentation using DIC images. This result is based on the inherent characteristics of Hoffman microscopy and the complex shape of cultured prostate cells. Hoffman microscopy is similar to DIC microscopy in that the images have the illusion of three-dimensionality (8). However, Hoffman images (Figs. 1, 4) are not as sharp or as detailed when compared to DIC images (Fig. 2). For example, in Hoffman images, the pseudopodal extensions and membrane ruffling seen in a living prostate cell appear either indistinct (Fig. 4a,c) or

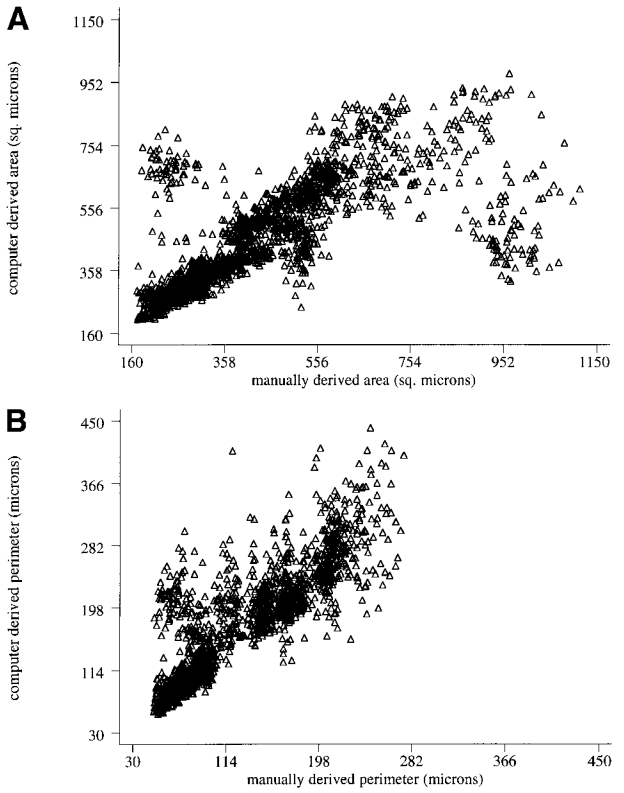

FIG. 3. **A:** Scatter plot comparing area measurements between computer-determined and manually-determined cell boundaries. **B:** Scatter plot comparing perimeter measurements between computer-determined and manually-determined cell boundaries.

faint (Fig. 4b,d), causing areas in or surrounding a cell image to have intensity values comparable to the image background. This lack of detail may be due to the inherent bias in sensitivity of Hoffman microscopy to optical density gradients normal to its aperture slit orientation (8).

The weaknesses of Hoffman microscopy led us to explore the use of DIC images in our segmentation scheme. A prostate cell's internal components, membrane, and pseudopods were clearly seen on DIC images with relatively greater sharpness and contrast to the image background (Fig. 2). DIC image clarity, combined with the added capability of our system to find cells close to an image edge, enabled our segmentation algorithm to detect cell boundaries with excellent precision in comparison to manual tracings (Fig. 5).

Scatter plot studies of morphometric features derived from DIC segmented cell images showed a strong linear correlation between manually- and computer-derived measurements (Fig. 3). One can see from Figure 3 that the segmentation algorithm had difficulty in accurately measuring only a small number of cells. After viewing the images corresponding to these outliers, we found that these cell images fell into two categories: cell images with a high ratio of background to image area (Fig. 6a), and cell images with very poor intensity contrast (Fig. 6b). Cell images

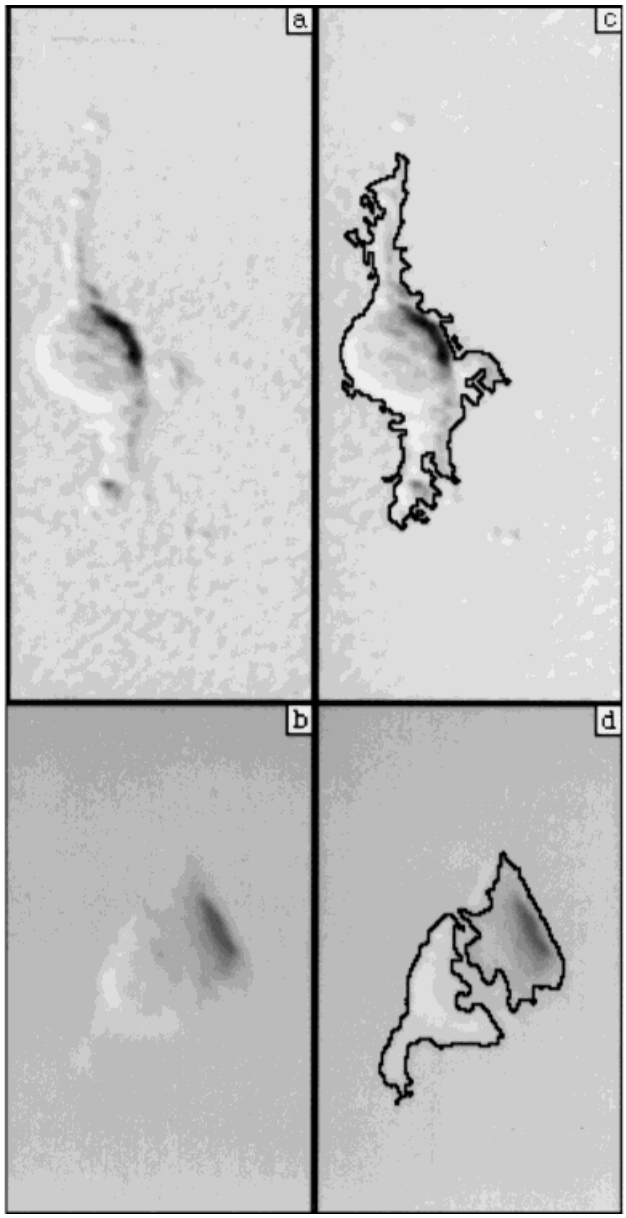

FIG. 4. **a,c:** Raw and computer-segmented Hoffman images, respectively, of a prostate cell with a complex shape. **b,d:** Raw and computer-segmented images, respectively, of a prostate cell with an indistinct shape.

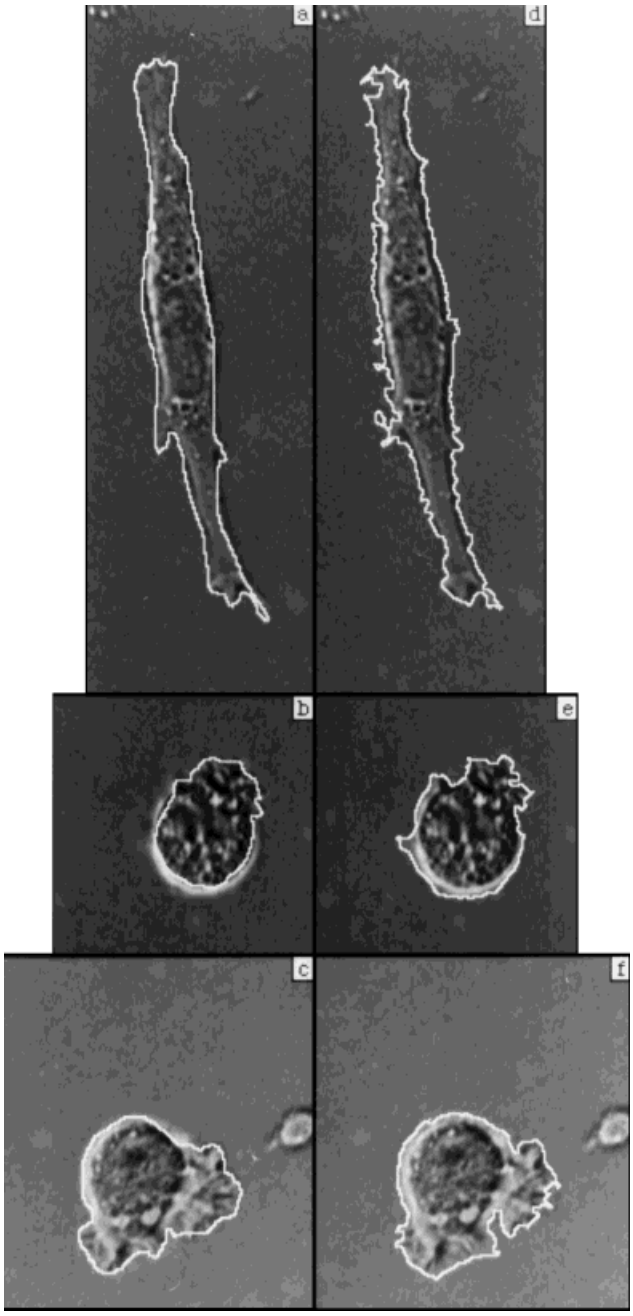

FIG. 5. **a–c:** DIC Cell images with manually-traced cell boundaries. **d–f:** Cell images with computer-determined cell boundaries.

with a high ratio of background to cell image area (Fig. 6a) had a large background area that artificially lowered the intensity at which areas were labeled as candidate cell regions during unipolar intensity transformation and global intensity thresholding. This bias resulted from the creation of a 64-image sequence large enough to accommodate the movement of the cell throughout the time period. As a consequence, a greater variation in background intensity and content was included that could affect segmentation. A possible method of eliminating this problem involves the creation of a movable region of interest around the cell; this approach is currently being evaluated. Cell images with poor intensity contrast were identified as those in which the average intensity of the cell border differed from the surrounding background by fewer than 4 grayscale levels. Analysis of our data showed that these images represented cells with very thin membranes (Fig. 6b). Thin cellular membranes, which can be easily traced by a manual operator, cannot be reliably detected by our segmentation algorithm because adequate intensity con-

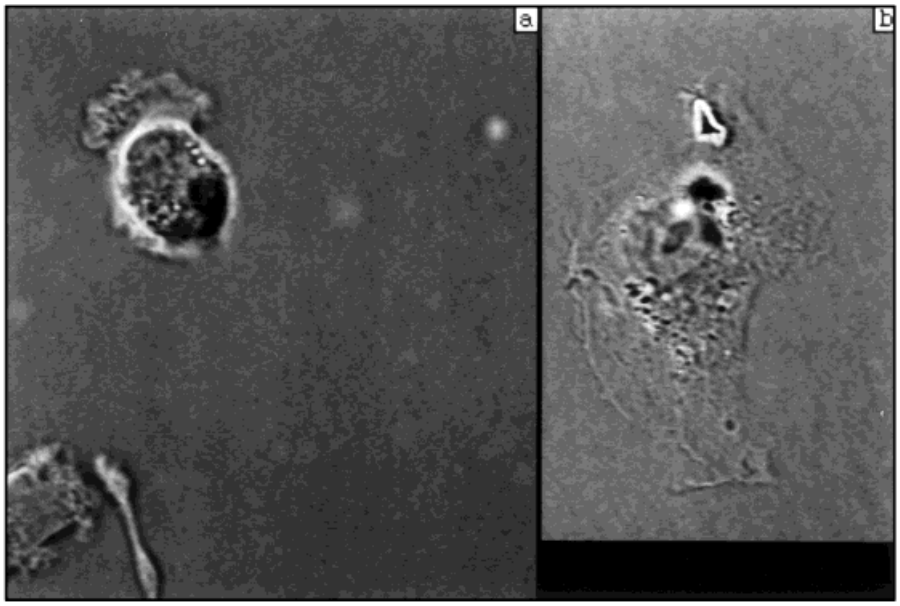

FIG. 6. **a:** DIC image having a high ratio of background to cell area. **b:** DIC image of cell with a thin membrane. The segmentation algorithm had difficulty segmenting images with poor intensity contrast and images having a high ratio of background to cell area.

trast between the cell and background is necessary for the segmentation algorithm to perform well. Other potential problems not addressed by our segmentation algorithm are: cells that move off the screen during image acquisition, poor focusing, and the need for user intervention in choosing cells to be imaged and analyzed.

The a priori exclusion of thin cells from the entire segmentation process sharply increases our ability to find cell boundaries that are accurate compared to manually traced cell boundaries, while removing only a fraction of cells available for segmentation analysis. The correlation between manually- and computer-derived area was 0.93, and between manually- and computer-derived perimeter length, 0.93. These results confirm that our segmentation algorithm can detect prostate cell outlines as effectively as other methods that require manual cell tracing. The added benefits of our segmentation system over manual tracing are its speed and its reproducibility of results. Our segmentation algorithm can determine cell boundaries in a 64-image sequence at least eight times faster than a manual operator. Furthermore, the segmentation algorithm will determine the same boundary for a cell regardless of the number of times it is presented to the system. This event is highly unlikely with a manual operator. Our segmentation algorithm is easily portable onto any computer having NIH Image, Version 1.60, a software package freely available on the internet (http://rsb.info.nih.gov/nih-image).

Motility studies that previously relied on time-intensive and inconsistent manual tracing can now be implemented using an efficient and reproducible segmentation algorithm. Integration of our segmentation algorithm in any image-analysis system using cell images should lead to improvements in system speed and consistency. Ongoing work in our laboratories involves the use of our segmentation algorithm in concert with the Fourier analysis system developed by Partin et al. (19) to quantify cell motility for estimation of metastatic potential in prostate cancer.

LITERATURE CITED

1. Brown DC, Gatter KC: Monoclonal antibody Ki-67: Its use in histopathology. Histopathology 17:489–503, 1990.
2. Chan KL: Quantitative characterization of electron micrograph image using fractal feature. IEEE Trans Biomed Eng 42:1033–1037, 1995.
3. Clements JD, Buzy JM: Automated image analysis for counting unstained cultured neurones. J Neurosci Methods 36:1–8, 1991.
4. Dejter SW Jr, Cunningham RE, Noguchi PD, Jones RV, Moul JW, McLeod DG, Lynch JH: Prognostic significance of DNA ploidy in carcinoma of prostate. Urology 33:361–366, 1989.
5. Gleason DF: Histological grading and clinical staging of prostate carcinoma. In: Urologic Pathology: The Prostate, Tannenbaum M (ed). Lea & Febinger, Philadelphia, 1977, pp. 171–197.
6. Gundlach H: Phase contrast and differential interference contrast instrumentation and applications in cell, developmental, and marine biology. Opt Eng 32:3223–3228, 1993.
7. Haralick R, Shapiro L: Image segmentation techniques. Comput Vis Graphics Image Processing 29:100–132, 1985.
8. Hoffman R, Gross L: Modulation contrast microscope. Appl Opt 14:1169–1176, 1975.
9. Lachney CL, Lonergan TA: Regulation of cell shape in *Euglena gracilis.* III. Involvement of stable microtubules. J Cell Sci 74:219–237, 1985.
10. Leitner F, Paillasson S, Ronot X, Demongeot J: Dynamic functional and structural analysis of living cells: New tools for vital staining of nuclear DNA and for characterization of cell motion. Acta Biotheor (Leiden) 43:299–317, 1995.
11. Lieberman SJ, Hamasaki T, Satir P: Ultrastructure and motion analysis of permeabilized paramecium capable of motility and regulation of motility. Cell Motil Cytoskeleton 9:73–84, 1988.
12. Mohler JL, Partin AW, Coffey DS: Prediction of metastatic potential by a new grading system of cell motility: Validation in the Dunning R-3327 prostatic adenocarcinoma model. J Urol 138:168–170, 1987.
13. Mohler JL, Partin AW, Isaacs JT, Coffey DS: Metastatic potential prediction by a visual grading system of cell motility: Prospective validation in the Dunning R-3327 prostatic adenocarcinoma model. Cancer Res 48:4312–4317, 1988.
14. Mohler JL, Partin AW, Isaacs WB, Coffey DS: Time lapse videomicroscopic identification of Dunning R-3327 adenocarcinoma and normal rat prostate cells. J Urol 137:544–547, 1987.
15. NIH Image Manual for public domain NIH Image program, U.S. National Institutes of Health, Bethesda, MD; available at http://rsb.info.nih.gov/nih-image.

16. American Cancer Society: Cancer Facts and Figures-1997. American Cancer Society Inc., Atlanta, 1997; p. 25.
17. Partin AW, Isaacs JT, Trieger B, Coffey DS: Early cell motility associated with an increase in metastatic ability in rat prostatic cancer cells transfected with the v-Harvey-*ras* oncogene. Cancer Res 48:6050–6053, 1988.
18. Partin AW, Mohler JL, Coffey DS: Cell motility as an index of metastatic ability in prostate cancers: Results with an animal model and with human cancer cells. In: Therapy for Genitourinary Cancer, Lepor H, Lawson RK (eds). Kluwer Academic Publishers, Hingham, MA, 1992, pp. 121–130.
19. Partin AW, Schoeniger JS, Mohler JL, Coffey DS: Fourier analysis of cell motility: Correlation of motility with metastatic potential. Proc Natl Acad Sci USA 86:1254–1258, 1989.
20. Partin AW: A quantitative analysis of tumor cell motility: Prostate cancer. Dissertation, Johns Hopkins University, Baltimore, 1988.
21. Poon SSS, Ward RK, Palcic B: Automated image detection and segmentation in blood smears. Cytometry 13:766–774, 1992.
22. Russ JC: The Image Processing Handbook, Ed. 2. CRC Press, Boca Raton, 1995, pp 165, 173–175, 347–349, 469–474.
23. Sahoo PK, Saltani AK, Wong AKC, Chen YC: A survey of thresholding techniques. Comput Vis Graphics Image Processing 41:233–260, 1988.
24. Soll D: The use of computers in understanding how animal cells move. Int Rev Cytol 163:43–104, 1995.
25. Thomas DJ, Robinson M, King P, Hasan T, Charlton R, Martin J, Carr TW, Neal DE: p53 expression and clinical outcome in prostate cancer. Br J Urol 72:778–781, 1993.
26. Veselý P, Lüers H, Riehle M, Bereiter-Hahn J: Subtraction scanning acoustic microscopy reveals motility domains in cells in vitro. Cell Motil Cytoskeleton 29:231–240, 1994.
27. Wu K, Gauthier D, Levine MD: Live cell image segmentation. IEEE Trans Biomed Eng 42:1–12, 1995.
28. Xu-van Opstal WY, Ranger C, Lejeune O, Forgez F, Boudin H, Bisconte JC, Rostene W: Automated image analyzing system for the quantitative study of living cells in culture. Microsc Res Tech 28:449–447, 1994.